Proppant transport in hydraulic fractures: computer simulation of effective properties and movement of the suspension

Vitaly A. Kuzkin Anton M. Krivtsov Aleksandr M. Linkov
kuzkinva@gmail.com

Abstract

The paper aims to develop approaches serving for adequate simulation of the proppant transport in hydraulic fractures. It is stated that prescribing proper rheology of the suspension at different proppant concentrations is of key significance. An attempt to replace expensive and time consuming physical measurements by numerical experiments is carried out. Two distinct computational methods, the particle dynamics (PD) and the smoothed particle hydrodynamics (SPH), are employed to complement each other and to verify the numerical results. We discuss theoretical rationale of the methods and the choice of appropriate input parameters for the problem under consideration. The calculations performed gave us the dependence of the suspension rheology on the proppant concentration. We could see that, when the number of degrees of freedom is high enough, the both methods provided close results. It is shown that in the case of the proppant suspended in a Newtonian fluid, the profile of the suspension velocity is parabolic in the range of volumetric proppant concentrations from 0 to 0.3. This implies that the suspension may be considered as a Newtonian fluid with the effective dynamic viscosity depending on the concentration. It appears that the dependence of the effective viscosity on the concentration becomes strongly non-linear when the concentration exceeds 0.15. A simple analytical equation approximating the dependence in the studied range of the proppant concentration is derived. Conclusions on further work are drawn.

1 Introduction

Hydraulic fracturing is a widespread technology used since the late 1940's for stimulation of oil and natural gas production [1]. A key process accompanying hydraulic fracturing is transport of proppant (small particles suspended in the fluid). The proppant serves to prevent the fracture closure after the pressure drop. The flow of the suspension strongly influences the fracture propagation. Consequently, proper accounting for the effective properties of the suspension is significant for reliable simulation of hydraulic fractures.

In practice, it is commonly assumed that the proppant-fluid mixture could be replaced by an equivalent single fluid (see, e.g. [2]). Rheological properties of the equivalent fluid (suspension) depend on the proppant concentration. In papers [3, 4, 5, 6] on the basis of experimental data it is proposed to consider three types of suspensions depending on the particle concentration c: dilute ($c < 0.02$), semi-dilute ($0.02 < c < 0.25$), and concentrated ($c > 0.25$). The dilute suspensions are Newtonian fluids with the viscosity μ_s

depending on proppant concentration according to the Einstein formula [7]:

$$\mu_s(c) = \mu_s(0)\,(1 + \beta c)\,, \tag{1}$$

where $\beta = 5/2$ in 3D, while $\beta = 2$ in 2D problems [8]. For a semi-dilute suspension, the Einstein formula is no longer accurate, as hydrodynamic interactions between particles become essential. Still the behavior of semi-dilute suspensions can be approximately considered as Newtonian [3, 4, 5, 6]. In concentrated suspensions, non-Newtonian effects are significant [3, 4, 5, 6, 9].

In this paper, dilute and semi-dilute suspensions are considered. For them, the rheology may be described by the dependence of the dynamic viscosity on the proppant concentration. A variety of models for this dependence is suggested in literature. According to the review [10], the majority of the models is derived either analytically or by fitting experimental data. Evidently each of the approaches has its limitations. Analytical models usually incorporate strong assumptions of limited applicability. The challenges of experimental techniques are described in the paper [6].

Consequently, computer simulations may play an important role as an additional tool for the investigation. The solution of Navier-Stockes equations for the suspension using conventional methods of computational fluid dynamics is extremely time-consuming. Therefore many alternative techniques, such as Stokesian Dynamics [11], Dissipative Particle Dynamics [12], Smoothed Particles Hydrodynamics [13], Molecular Dynamics [14], Lattice Boltzmann [15, 16], etc., are used in literature for simulation of suspensions. In the present paper, the particle dynamics [17, 18, 19] and smoothed particles hydrodynamics (SPH) [20, 21] are used. These methods mutually complement each other. Particle dynamics is simple and contains small number of parameters. However in the framework of the particle dynamics a viscosity can not be specified explicitly. In smoothed particles hydrodynamics viscosity is a parameter of the model. At the same time the motion of smoothed particles is less intuitive and in some cases even artificial [21]. Therefore the joint use of these methods may serve for better understanding of the suspension behavior and verifying the results.

In the present paper, the particle dynamics and smoothed particle hydrodynamics are employed for simulation of the proppant-fluid flow in a narrow channel. Proppant concentrations in the range $[0; 0.3]$ are considered. The theoretical rationale for modeling is presented in the section 2. Formulas relating characteristics of the flow with rheological properties of the suspension are derived. Simulation techniques are described in the section 3. The results of simulations using the both methods are given in the section 4.

2 Analytical solution for steady flow of a viscous fluid in a narrow channel

In accordance with the assumption used for simulation of hydraulic fractures in practice, we assume the slurry to be a viscous fluid with properties depending on the proppant concentration. Thus the stress tensor σ is represented as $\sigma = -p\mathbf{E} + \tau$, where p is the pressure ($p \geq 0$), $\mathbf{E}$ is the unit tensor, τ is the deviatory part of the stress tensor depending on the strain rate tensor $\dot{\varepsilon}$. The viscosity law, defining the dependence of τ on the proppant concentration is to be found from numerical experiments.

Firstly, we employ general considerations, commonly used when deriving the Poiseuille equation for a flow in a narrow channel. Specifically, we assume that the channel width w is much less than the characteristic length of the fluid flow in the channel's plane. This allows

one to neglect the flow across the width and to consider the pressure constant through the width. The pressure gradient is assumed constant in the direction x of the fluid flow: $\frac{\partial p}{\partial x} = -j_p$. Then in steady-state regime the equations of the motion reduce to the only equation:

$$\frac{\partial \tau_{xy}}{\partial y} = -j_p - \rho f_x, \tag{2}$$

where y is the axis normal to the flow plane, ρ is the mass density, f_x is the body force in the direction of the flow. Without loss of generality, we may include the pressure change per unit length into the body force, writing the equation as

$$\frac{\partial \tau_{xy}}{\partial y} = -f_p, \tag{3}$$

where $f_p = j_p + \rho f_x$. This interpretations will also serve us in numerical experiments to simulate the pressure gradient by an equivalent body force. Locating the y-axis in the middle plane of the channel and integrating (3) along this axis, we obtain the following distribution of the shear stress across the channel:

$$\tau_{xy}(y) = -f_p y, \tag{4}$$

where we have taken into account that $\tau_{xy}(0) = 0$ by symmetry.

Under the assumptions accepted, the only nonzero component of the shear strain rate is $\dot{\varepsilon}_{xy} = \dot{\gamma}/2$, where $\dot{\gamma} = \frac{\partial v_x}{\partial y}$. Hence for the considered flow, the general form of the viscosity law is:

$$\tau_{xy} = F(\dot{\gamma}), \tag{5}$$

where the function $F(\dot{\gamma})$ is to be found from physical or numerical experiments. The inverse function $\dot{\gamma} = F^{-1}(\tau_{xy})$ defines the derivative $\frac{\partial v_x}{\partial y}$ as a function of the shear stress τ_{xy}. Then the equation (4) completely defines this derivative: $\frac{\partial v_x}{\partial y} = F^{-1}(-f_p y)$, and integration with respect to y under the boundary condition $v_x(w/2) = 0$, gives

$$v_x(y) = \int_{\frac{w}{2}}^{y} F^{-1}(-f_p y)dy. \tag{6}$$

From now on, to simplify notations, we omit the subscript x in the velocity v_x. From (6), we have for the maximal velocity $v_m = v(0)$ and for the average velocity $v_{av} = \frac{2}{w}\int_0^{\frac{w}{2}} v_x(y)dy$:

$$v_m = \int_{\frac{w}{2}}^{0} F^{-1}(-f_p y)dy, \quad v_{av} = \frac{2}{w}\int_0^{\frac{w}{2}} \left[\int_{\frac{w}{2}}^{y} F^{-1}(-f_p y)dy\right] dy. \tag{7}$$

In practice, it is convenient to approximate the viscosity function $F(\dot{\gamma})$ by the power-type dependence:

$$F(\dot{\gamma}) = M\dot{\gamma}^n, \tag{8}$$

where M and n are called the consistency index and the behavior index, respectively. For a Newtonian fluid ($n = 1$), $M = \mu$ is the dynamic viscosity; for a perfectly plastic fluid ($n = 0$), $M = \tau_0$ is the shear strength.

Under the approximation (8), $F^{-1}(\tau_{xy}) = (\tau_{xy}/M)^{1/n}$. Then integration with respect to y in (6) yields:

$$v(y) = v_m \left[1 - \left(\frac{2y}{w}\right)^{\frac{n+1}{n}}\right], \qquad v_m = \frac{n}{n+1}\frac{w}{2}\left(\frac{f_p w}{2M}\right)^{\frac{1}{n}}. \tag{9}$$

The average velocity is

$$v_{av} = \frac{n}{2n+1}\frac{w}{2}\left(\frac{f_p w}{2M}\right)^{\frac{1}{n}}. \tag{10}$$

Let us rewrite (10) as

$$f_p = M_p v_{av}^n, \quad M_p \stackrel{\text{def}}{=} M\frac{(2+1/n)^n}{(w/2)^{n+1}}, \tag{11}$$

where M_p may be called the generalized consistency factor. Comparison of the equation (11) with (8) shows that the solution for the Poiseuille type flow actually translates the viscosity law (8) in terms of the shear stress and the shear strain rate into the analogous dependence (11) between the pressure gradient and the average velocity. Notably, the generalized consistency factor M_p is proportional to M. Still M_p depends also on the behavior index n. Specifically, when measuring the length in the units of the half-width $w/2$, we have $M_p = M(2+1/n)^n$. Then for a Newtonian fluid, $M_p = 3M = 3\mu$; for a perfectly plastic fluid, $M_p = M = \tau_0$.

From (9), it is clear that for a Newtonian fluid, the profile is parabolic. Hence, as far as simulations of a suspension movement lead to the velocity profile, which is parabolic to an accepted accuracy, the considered suspension may be assumed Newtonian. In this case, the equation (10) for the average velocity, may serve to find the effective viscosity μ_s:

$$\mu_s = \frac{f_p w^2}{12 v_{av}}. \tag{12}$$

In cases, when the profile cannot be approximated by a parabolic dependence, the behavior and consistency indices are found by matching (11) with experimental data on the dependence of the average velocity on the pressure gradient. To this end, it is convenient to re-write (11) in log-log coordinates as

$$\ln v_{av} = C + A\ln f_p, \qquad C = -\ln(2+A) + (1+A)\ln\frac{w}{2} - A\ln M, \qquad A = \frac{1}{n}. \tag{13}$$

Then the slope A of the plot $\ln v_{av}$ against $\ln f_p$ provides the behavior index $n = 1/A$. After this, the expression for C defines the consistency index M.

Thus if the dependence of the mean velocity of the suspension on the body force is found from physical or numerical experiments, then the rheological properties of the suspension are calculated using either formula (12) or formula (13). This approach is used in section 4 for interpretation of the results of computer simulations.

3 Simulation technique

Let us summarize the general statement of the problem considered in the present paper. The flow of Newtonian fluid containing proppant particles in a channel of constant width is considered. The channel is simulated by a square computational domain with periodic

boundary conditions [18] in the direction of the flow and rigid walls in the orthogonal direction. The flow is driven by the constant body force acting along the flow. As explained in the previous section, this statement is equivalent to the flow under constant pressure gradient, while the implementation of the body force is notably simpler. The initial conditions correspond to the Poiseuille flow of a single Newtonian fluid. As the presence of proppant changes the rheological properties of the suspension (increases the viscosity) the initial parabolic velocity profile is decaying until the steady-state regime is reached. The velocity profile in the steady-state regime is used for estimating the rheological properties of the suspension. The problem is solved using two numerical methods, notably particle dynamics [17, 18, 19] and smoothed particle hydrodynamics [20, 21]. Detailed description of the simulation techniques is given below.

3.1 Particle Dynamics: the multisphere approach

In the framework of particle dynamics method [17, 18, 19], the fluid is represented by the set of interacting particles (material points). Classical Newtonian equations of motion for the particles are solved numerically. In the present paper leap-frog integration scheme [18] is used. Inter particle interactions are described by spline potential [19]. The force acting between particles i and j is calculated using the following formula:

$$\mathbf{F}_{ij} = \frac{fk(r_{ij})}{a}\left[\left(\frac{a}{r_{ij}}\right)^{13} - \left(\frac{a}{r_{ij}}\right)^{7}\right]\mathbf{r}_{ij},$$

$$k(r) = \begin{cases} 1, & r \le b \\ \left(1 - \left(\dfrac{r^2 - b^2}{a_{cut}^2 - b^2}\right)^2\right)^2, & b < r < a_{cut}, \\ 0, & r \ge a_{cut} \end{cases} \tag{14}$$

where a_{cut} is a cut-off radius, a is an equilibrium distance between particles, f is a force constant, $b = \left(13/7\right)^{1/6} a$.

Proppant particles are simulated as follows. Every proppant particle is represented as a set of rigidly connected smaller particles as it is shown in figure 1. Thus each proppant particle is a rigid body with two translational and one rotational degrees of freedom. The distance between the nearest particles for the outer circle is equal to the equilibrium

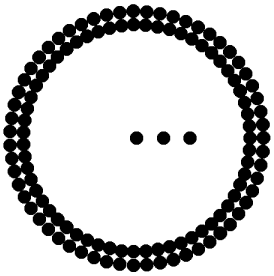

Figure 1: Multisphere representation of a proppant particle. Three particles in the middle are used for visualization of particle orientation.

distance a between fluid particles. The distance between inner and outer circles is also equal

to a. These particles interacts with fluid particles via the forces defined by formula (14). Note that the interactions with fluid cause both translation and rotation of proppant particles. Thus the equations of motion of proppant particle i have the form

$$m_p\dot{\mathbf{v}}_i = \sum_{k\in\Lambda_i}\sum_{j\neq i, j\notin\Lambda_i}\mathbf{F}_{kj} + m_p\mathbf{g}, \quad \Theta_p\dot{\varphi}_i = \sum_{k\in\Lambda_i}\sum_{j\neq i, j\notin\Lambda_i}(\mathbf{r}_k - \mathbf{r}_i)\times\mathbf{F}_{kj}, \tag{15}$$

where m_p is the mass of a proppant particle; φ_i is the angle describing the orientation for i-th proppant particle; Λ_i is the set of indices for the particles representing the proppant particle i; Θ_p is the moment of inertia of the proppant particle with respect to the center of mass; $\mathbf{g}$ is the body force driving the flow. The approach for simulation of proppant particles described above is similar to the so-called multisphere approach [22, 23], widely used in the framework of Discrete Element Method [24]. Usually the multisphere approach is applied for description of interactions between non-spherical particles of complex shape. Though the proppant particles in the present paper are spherical, the multisphere approach is still computationally more efficient than the straightforward approach, when the proppant particles are represented by large spheres. The better efficiency of multisphere method is explained as follows. In PD simulations, evaluation of forces employs dividing the computational domain is divided into cells with the size equal to the cut-off radius [19]. It serves for considering only the particles in neighboring cells instead of taking into account all particles in the computational domain. The multisphere approach uses the cells with the size equal to cut-off distance for the fluid particles. Thus execution times for systems with and without proppant are almost identical.[1] At the same time if the proppant particles are represented by large spheres, then the computational cell size is equal to the radius of the sphere plus the cut-off radius for proppant-fluid interactions. In the latter case the cell size is much larger and hence the cell contains larger number of fluid particles. Therefore the execution time is greater. The solution of test problems has shown that the multisphere approach is almost one order faster for $R/a = 3$, where R is a proppant radius. Thus the multisphere approach is useful for simulation of particles of significantly different sizes.

The flow in a narrow channel with constant width is simulated as follows. The square computational domain is considered. The rigid walls are simulated using two rows of fixed fluid particles. Periodic boundary conditions [18] are applied in the direction of the flow. As the work done by shear stresses causes heating of the fluid, the generated heat should be extracted from the system. The Berendsen thermostat [25] is used for this purpose. The thermostat is applied to the narrow stripe of the fluid near the left boundary of the computational domain. The width of the stripe is $5a$. In this case the heated fluid leaving the domain to the right is cooled down by the thermostat after crossing the periodic boundary. The thermostat algorithm is the following. The velocity profile is calculated. For this purpose the domain is divided into stripes with the width equal to a_{cut}. The stream velocity for the stripe is equal to the average velocity of the particles inside the stripe. For the application of Berendsen thermostat the stream velocities are subtracted from the particle velocities. The remaining "thermal" velocities are multiplied by the following scaling coefficient:

$$k = \sqrt{\frac{K_0}{K_a}}, \qquad K_a = \frac{1}{2}m\sum_i(\mathbf{v}_i - \mathbf{v}(\mathbf{r}_i))^2, \tag{16}$$

[1]The execution time decreases with proppant concentration, because the proppant particles are represented only by the particles on the surface. Thus the total number of particles used in simulation decreases.

where K_0 is a desired value of the thermal kinetic energy of the fluid; $\mathbf{v}(\mathbf{r}_i)$ is the stream velocity at the point, where the i-th particle is located. As a result, the heat generated by the shear flow is removed from the system and the viscosity of the fluid is constant.

3.2 Smoothed Particles Hydrodynamics

The second method used in the present paper for simulation of proppant transport is Smoothed Particles Hydrodynamics (SPH) [20, 21]. Similarly to particle dynamics, the fluid is represented by a set of interacting particles. The motion of the particles is governed by the following equations

$$\dot{\mathbf{v}}_i = -\sum_j m\left(\frac{p_i}{\rho_i^2} + \frac{p_j}{\rho_j^2} + S_{ij}\right)\psi'(r_{ij})\mathbf{e}_{ij} + \mathbf{g}, \quad \rho_i = \sum_j m\psi(r_{ij}), \tag{17}$$

where p_i, ρ_i are, respectively, the pressure and the density at the point, where the particle i is located; S_{ij} is a viscous term; ψ is a weighting or kernel function [20]. The weighting function $\psi(r)$ has a compact support, vanishing for $r \geq a_{cut}$, where a_{cut} is a smoothing length identical to the cut-off radius used in the particle dynamics method. In the following calculations, Lucy weighting function is used [20]:

$$\psi(r) = \frac{5}{\pi a_{cut}^2}\left(1 + 3\frac{r}{a_{cut}}\right)\left(1 - \frac{r}{a_{cut}}\right)^3, \quad r \in [0; a_{cut}]\,. \tag{18}$$

The following constitutive relations, proposed by Monaghan [20], for the pressure and the viscous term are used

$$p_i = B\left(\left(\frac{\rho_i}{\rho_0}\right)^\gamma - 1\right), \quad S_{ij} = -\frac{16\mu_i\mu_j}{\rho_i\rho_j(\mu_i+\mu_j)}\frac{\mathbf{v}_{ij}\cdot\mathbf{r}_{ij}}{r_{ij}^2 + \epsilon a^2}, \quad \mu_i = \frac{1}{8}\alpha a_{cut} v_s \rho_i, \tag{19}$$

where ρ_0 is an equilibrium fluid density; $B, \alpha, \gamma, \epsilon$ are parameters of the model; a is a characteristic size of the particle; v_s is the speed of sound. In the paper [20] it is shown that the equation of state for pressure in form (19) guarantees low compressibility of the fluid. In contrast to particle dynamics, where viscosity arises naturally as a result of stochastic motion, in SPH the viscosity is introduced explicitly as the key parameter of the model. Additionally the following purely repulsive core potential is used for preventing the formation of artificial structures in the fluid [21]:

$$\Phi_{core}(r) = \frac{f a_{core}}{4}\left(1 - \frac{r^2}{a_{core}^2}\right)^4, \tag{20}$$

where a_{core} is a cut-off radius for the core potential. Interactions between proppant particles, as well as between proppant and fluid particles are described by using formula (14). For proppant-proppant interactions the forces are truncated at $r = a$, hence the interactions are purely repulsive.

In the simulations discussed below, the following boundary conditions are used. A square computational domain is considered. Its rigid walls are simulated using two rows of fixed fluid particles. Periodic boundary conditions are applied in the direction of the flow. The standard implementation of periodic boundary conditions is employed [18].

3.3 Scaling of the parameters

In the particle dynamics method, as well as in many other numerical methods, the fluid is represented by a discrete system with a finite number of degrees of freedom. Evidently the results depend on this number. There are two reasons for the dependence of the results on the number of particles. The first is that the definitions of continuum properties for a discrete system containing relatively small number of particles are ambiguous. This problem is described in more details in the paper [26]. In particular, it is shown that the mechanical characteristics of the system depend on the number of particles in the system. In the present paper this dependence is not significant, because the number of particles used is quite large.

The second reason is the dependence of microscopic parameters (parameters of discrete system) on the number of particles. Consider two discrete systems with different number of particles N_0 and N_1 corresponding to the same square specimen of the fluid. Let us derive the relation between parameters of these discrete systems. In particular, if a_0 is a reference equilibrium distance, then the size of the fluid specimen is equal to $\sqrt{N_0}a_0$. Since the size of the system does not depend on the number of particles, the equilibrium distances a_0 and a_1 for the two discrete systems are related as:

$$a_1 = \sqrt{\frac{N_0}{N_1}}a_0. \tag{21}$$

Assuming the fluid density and the sound speed $v_s = \sqrt{6fa/m}$ constant, one obtains:

$$m_1 = \frac{N_0}{N_1}m_0, \qquad f_1 = \sqrt{\frac{N_0}{N_1}}f_0. \tag{22}$$

Let us derive analogous relation for the fluid viscosity. According to Chapman-Enskog theory, the gas viscosity in 2D can be represented as follows [27]

$$\mu \sim \frac{\sqrt{k_B T m}}{a}, \tag{23}$$

where k_B is the Boltzman constant, T is the temperature of the system. The characteristic temperature of a system is proportional to $mv_d^2/2$, where v_d is a dissociation velocity. Thus

$$\mu \sim \frac{mv_d}{a}. \tag{24}$$

Substituting formulas (21), (22) into formula (24) and taking into account that v_d does not depend on N_0/N_1, one obtains the following dependence of viscosity on the number of particles

$$\mu_1 \sim \sqrt{\frac{N_0}{N_1}}\mu_0. \tag{25}$$

Note that an analogous relation can be derived from the simple dimensional analysis:

$$\tau \sim \frac{f}{a}, \quad \dot{\gamma} \sim \frac{1}{t_*} \to \mu \sim \frac{ft_*}{a} \to \mu_1 \sim \sqrt{\frac{N_0}{N_1}}\mu_0, \qquad t_* = 2\pi\sqrt{ma/6f} \tag{26}$$

where t_* is the period of small oscillations for a single Lennard-Jones oscillator. Thus the viscosity of the system decreases with increasing resolution (number of particles). The dependence of the viscosity on the number of particles can not be avoided. However one

can avoid the analogous dependence for Reynolds number. Consider Reynolds number in the case of Poiseuille flow under the action of constant body force g:

$$\mathrm{Re} = \frac{\rho v_{max} w}{\mu} = \frac{\rho^2 g w^3}{8\mu^2}, \tag{27}$$

where the characteristic velocity v_{max} is defined by formula (9). Since the viscosity decreases with resolution, the Reynolds number increases. Let us choose the body force so that Reynolds number would remain constant in simulations with different resolution. Using formulas (25), (27) it is straightforward to show that the body force should have the form

$$g_1 = \frac{N_0}{N_1} g_0. \tag{28}$$

Thus the procedure described above allows us to avoid the dependence of the main parameters of the problem (size, density, sound speed, and Reynolds number) on the total number of particles in the system. In the case of SPH the scaling is more straightforward. The smoothing length and mass of the particles are scaled in accordance with formulas analogous to formulas (21), (22). The viscosity is introduced explicitly, hence in contrast to PD, no scaling is required in order to keep the viscosity independent on the number of particles.

4 Simulation of the influence of proppant on fluid flow in cracks induced by hydraulic fracturing

In this section we investigate the influence of proppant on rheological properties of the suspension. The most widespread size of proppant particles is 20/40 mesh or $0.004 - 0.008\ m$. The opening of the crack is of order of $0.01\ m$. Let us estimate the typical Reynolds number for hydraulic fracturing. Assume that water is used as proppant-transporting fluid. The density and dynamic viscosity of the water at normal conditions are 1000 kg/m^3 and 0.0009 Pa$\cdot s$. The characteristic velocity of the flow is $0.01\ m/s$. Therefore the typical Reynolds number is of order of 1. Note that this number should not be fitted exactly in computer simulations. The only requirement for the simulation is that the flow is laminar. Therefore one order higher Reynolds numbers are used in the present paper in order to speed up the simulations. Consider PD and SPH simulations of the proppant-fluid flow in the channel under the action of body force. A square computational domain under periodic boundary conditions in the direction of the flow and rigid walls in the orthogonal direction is considered. The initial conditions are as follows. In both cases the fluid particles initially form a perfect square lattice with nearest neighbor distances equal to a_0. Proppant particles are set randomly with uniform spatial distribution. The volumetric concentration of proppant particles is [16]

$$c = \frac{\pi R^2 N_p}{w^2}, \tag{29}$$

where w is the size of the computational domain; N_p is the total number of proppant particles. Proppant concentrations in the range [0;0.3] are considered. The boundary conditions are described above. In the case of PD simulations, the initial velocities of the fluid and proppant particles are set in accordance with the velocity profile given by formula (9) for $n = 1$. The uniformly distributed random velocities are added to achieve liquid state of the system. The particles are mixing rapidly and no additional preparations are required (see figure 2).

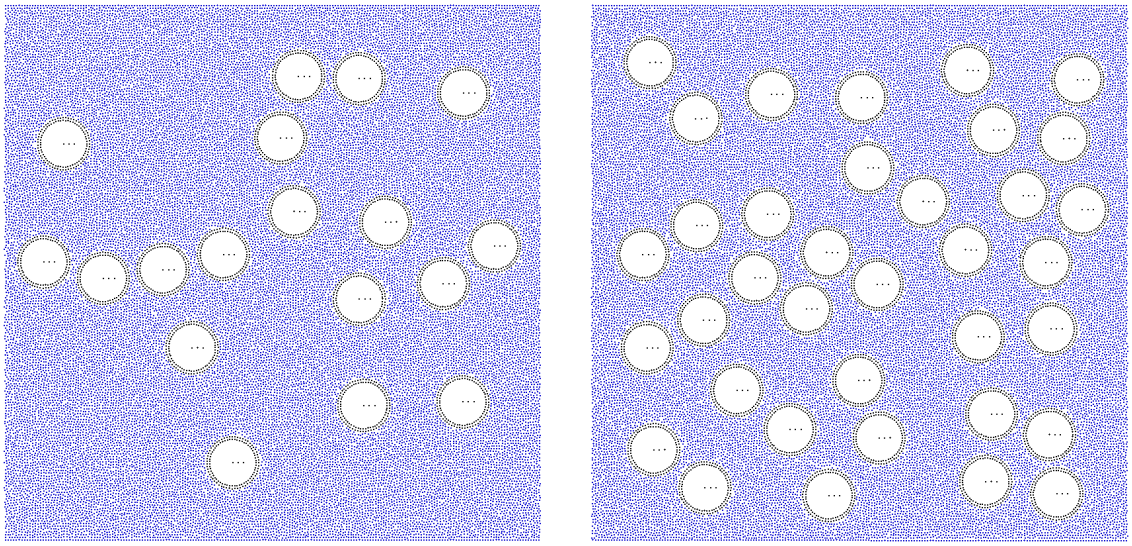

Figure 2: The distribution of fluid and proppant particles after 50 time steps of particle dynamics simulation. Proppant concentrations are 0.15 (left) and 0.3 (right).

In the case of SPH, the creation of initial configuration is not so straightforward. The fluid described by equation of state (19) is nearly incompressible. Therefore the computational domain should be completely filled by the particles. Otherwise the system would contain artificial voids, similar to gas bubbles. Complicated meshing strategies could be used in order to create uniform distribution of particles in the computational domain. However in the present paper, instead of using meshing algorithms, the following equilibration procedure is used. Proppant particles are randomly distributed in the computational domain. The remaining space is filled by fluid particles forming perfect square lattice. Evidently in this case some voids are formed around proppant particles. In order to remove the voids the system is compressed by multiplying equilibrium density ρ_0 by 0.8. After that, the density is slowly increased until the pressure in the system reaches the value of $0.01\ K$, where K is the bulk modulus of the fluid. In the course of this procedure the fluid and proppant particles move in accordance with the equations of motion described above. The resulting distribution of particles after equilibration is shown in figure 3. One can see that the computational domain is completely filled by the particles and no significant artifacts are present. After the equilibration particle velocities are set in accordance with parabolic velocity profile corresponding to the Poiseuille flow. The influence of the proppant concentration on the rheology of the suspension is investigated as follows. Computer simulations of the flow described above are carried out using particle dynamics and smoothed particles hydrodynamics. The following values of parameters are used in the framework of the both methods

$$\begin{aligned} &\frac{R}{w} = \frac{1}{20}, \quad \rho_f = 1, \quad \rho_p = 2, \quad \mathrm{Re} \approx 30, \quad v_s = 2.45, \quad m = 0.09 \\ &a = 0.3, \quad f = 0.3, \quad N = 4 \cdot 10^4, \quad s_{av} = 16666, \quad s_{max} = 2 \cdot 10^6, \end{aligned} \tag{30}$$

where ρ_f, ρ_p are the fluid and proppant densities, respectively; N is an approximate total number of particles; s_{av} is the number of time steps used for temporal averaging of the

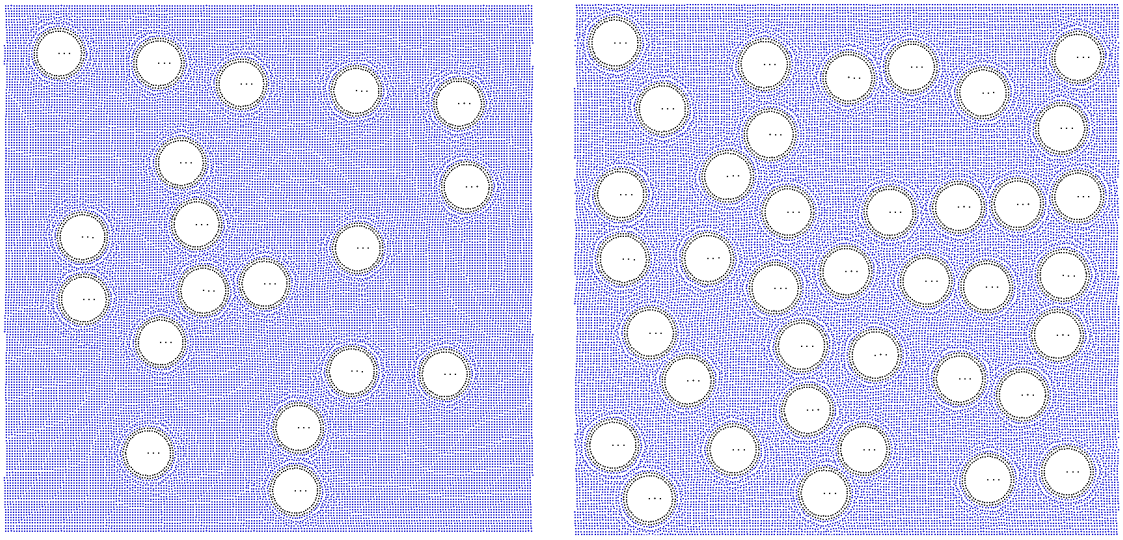

Figure 3: The distribution of smoothed (fluid) and proppant particles after equilibration. Proppant concentrations are 0.15 (left) and 0.3 (right).

results. The specific values of the parameters used in particle dynamics simulations are:

$$\begin{aligned} &\frac{T}{D} = 1.5, \quad \frac{a_{cut}}{a} = 2.1, \quad \frac{\Delta t}{t_*} = 0.01, \quad \frac{a_0}{a} = 0.98, \\ &\frac{v_0}{v_s} = 0.14, \quad \frac{mg}{f} = 2.58 \cdot 10^{-5}. \end{aligned} \tag{31}$$

where Δt is the time step; t_* is defined by formula (26). In SPH simulations, the parameters are set as follows:

$$\begin{aligned} &\frac{K}{\rho_0 v_s^2} = \frac{1}{7}, \quad \gamma = 7, \quad \frac{\beta}{a_{cut} v_s} = 0.23, \quad \frac{a_{cut}}{a} = 2.5, \quad \epsilon = 10^{-3}, \\ &\frac{\Delta t}{t_*} = 0.02, \quad \frac{a_0}{a} = 1, \quad \frac{v_0}{v_s} = 0.01, \quad \frac{mg}{f} = 6 \cdot 10^{-5}. \end{aligned} \tag{32}$$

In the both cases the velocity of the center of mass of all particles inside the computational domain is calculated during the simulation. Note that in a steady-state regime this velocity is identical to average profile velocity. A typical behavior of the velocity in PD and SPH simulations is shown in figure 4. On can see that the velocity decreases until the steady-state is reached. Note that in the steady-state regime the average velocity is still fluctuating because of rearrangements of proppant particles. The rearrangements occur, because the proppant particles closer to the center of the channel have larger velocities than those closer to the walls. Let us check if the suspension shows non-Newtonian behavior in the range of proppant concentrations considered in the present paper. As shown in section 2, it can be done via the analysis of the velocity profile in the steady-state regime. Consider velocity profiles at different proppant concentrations. The profile is calculated as follows. The computational domain is divided into equal layers parallel to the direction of the flow. The average velocity of particles in each layer is calculated. The resulting values are additionally time averaged. The profiles obtained in computer simulations using PD and SPH methods are shown in figure 5. One can see from figure 5 that the deviation of the velocity profiles form parabolic shape are relatively small. The deviations are caused

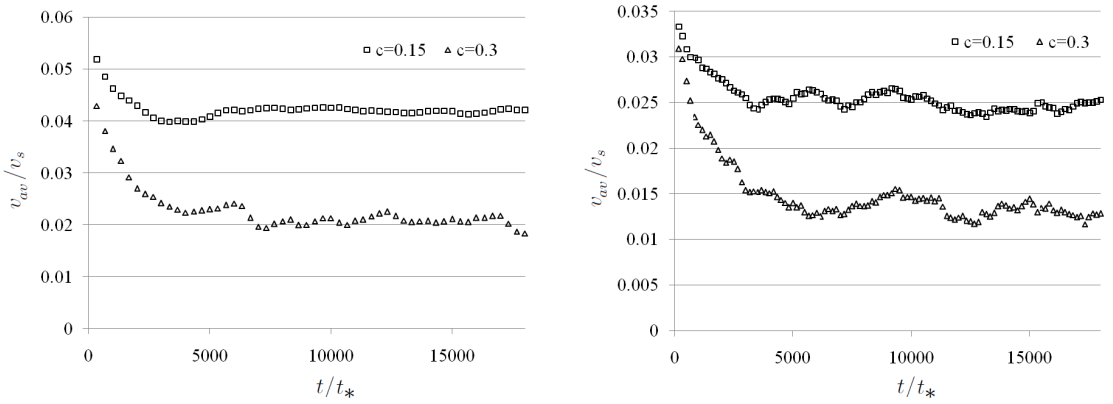

Figure 4: The evolution of the center of mass velocity for SPH (left) and PD (right) at proppant concentrations 0.15, 0.3.

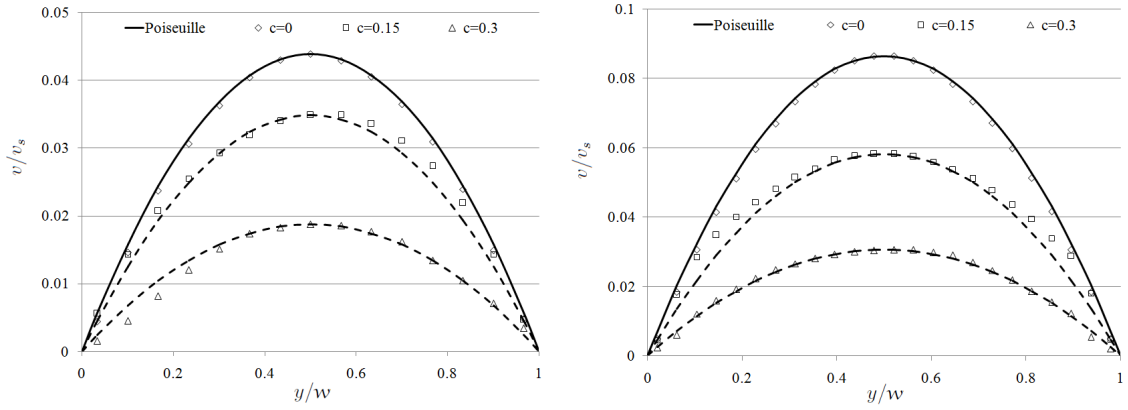

Figure 5: Velocity profiles at different proppant concentrations obtained using PD (left) and SPH (right). Dashed lines are parabolas with the same maximum value as the results of simulations.

by statistical fluctuations and non-uniform distribution of proppant particles in the computational domain. In particular, the latter reason leads to slightly non-symmetric velocity profile (see the graph corresponding to PD results with $c = 0.3$). Therefore for proppant concentrations in the range $[0; 0.3]$ the suspension can be considered as a Newtonian fluid. Note that the highest concentration $c = 0.3$ considered in the present paper is outside the range $[0.02; 0.25]$, corresponding to semi-dilute suspensions (according to classification presented in paper [6]). However it should be taken into account that in two dimensions, the critical concentration ($c_*^{2D} \approx 0.9$) is higher than in three dimensions ($c_*^{3D} \in [0.64; 0.74]$)[2]. Therefore the range of concentrations corresponding to semi-dilute suspensions in 2D is wider than in 3D.

Thus once non-Newtonian effects are negligible, one can calculate the effective viscosity of the suspension by using formula (12). Note that the density of the suspension in

[2]The value 0.64 corresponds to so-called Random Close-Packed lattice, while 0.74 corresponds to Face Centered Cubic. See paper [6] for more details.

formula (12) should be calculated as follows

$$\rho_s = \frac{mN_f + m_p N_p}{w^2}. \tag{33}$$

Note that density of the suspension depends on the proppant concentration. In computer simulations the body force was renormalized so that $\rho_s g$ does not depend on the proppant concentration. In this case the only parameter in formula (12) depending on the proppant concentration is the average velocity v_{av}. This value is obtained in computer simulations. Viscosity of the suspension, calculated for different proppant concentrations and the results of simulations are shown in figure 6. Every point on the plot is the mean of 5 simulations

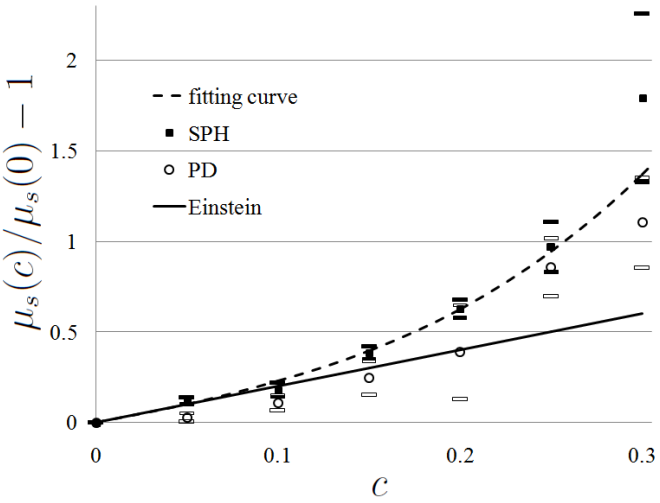

Figure 6: The dependence of relative viscosity on proppant concentration obtained using SPH and PD.

with different initial proppant distributions. The bars on the plot show the dispersion of the results (average value plus/minus standard deviation). The solid line corresponds to Einstein formula adopted for the 2D case in paper [8], the dashed line corresponds to the following fitting curve:

$$\mu_s(c) = \mu_s(0)\left(1 + 2c + 28.5c^3\right). \tag{34}$$

One can see from figure 6 that the difference between the results of PD and SPH simulations is of order of dispersion of PD results. For proppant concentrations higher than 0.15, the obtained values of the suspension viscosity are higher than the value predicted by the Einstein formula [8]. Therefore at these concentrations the hydrodynamic interactions between proppant particles, neglected in Einstein's derivation, are significant.

Finally, we need to check if the results depend on the number of particles used for discretization. The dependencies of the relative viscosity on the proppant concentration, obtained using PD and SPH with different number of particles, are shown in figure 7. The circles correspond to the results of single simulation and the squares are the values averaged over 5 simulations. One can see from figure 7 that two-fold increase of the particle number does not change the results significantly. This implies that the convergence with respect to the particle number is reached.

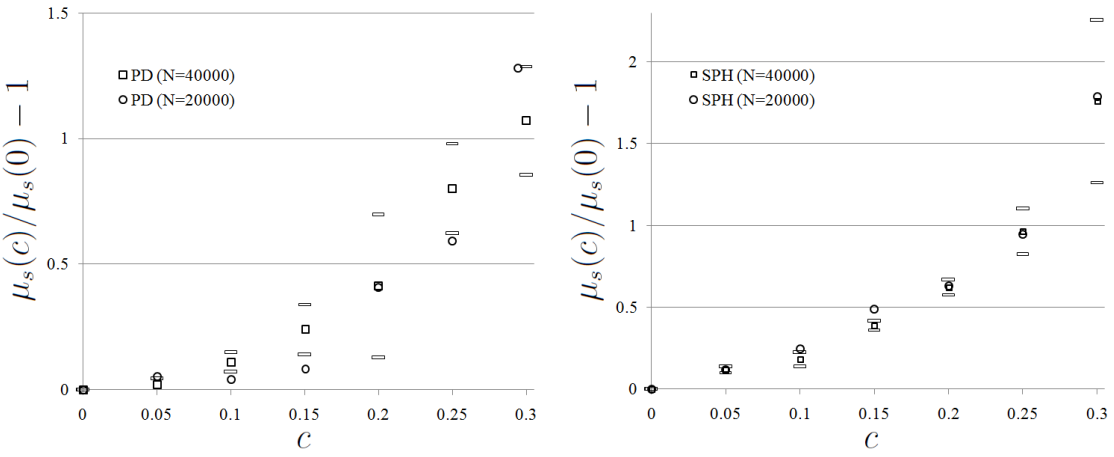

Figure 7: The dependence of relative viscosity on the proppant concentration obtained for different number of particles. Note that circles correspond to the result of single simulation, while squares represent the means over 5 simulations.

5 Summary

In the present paper the influence of proppant on the flow in a narrow channel was simulated by using particle dynamics and smoothed particles hydrodynamics methods. Steady-state Poiseuille-like flow was considered. Velocity profiles were obtained by the both methods. The simulations show that the profiles are parabolic for proppant concentrations in the range [0; 0.3]. Thus in this range, the suspension can be considered as semi-dilute [6], i.e. the viscosity of the suspension nonlinearly depends on the concentration, while non-Newtonian effects are negligible. It was established that the results of PD and SPH simulations agree to the accuracy of standard deviation. The dependence of the effective viscosity of the suspension on proppant concentration was obtained. For $c < 0.15$, the dependence is close to the Einstein formula, while for $c > 0.15$, the dependence is nonlinear and may be approximated by cubic polynomial. In further work, the analytical and computational techniques, developed in the present paper, will be used for simulation of suspension rheology at higher proppant concentrations ($c > 0.3$). Rheological parameters of the suspension (behavior n and consistency M indexes) will be calculated by modeling of Poiseuille flow and comparison of the results with the analytical relation (13) between the flux and the body force.

Acknowledgements

The authors are deeply grateful to Dr. A. Lavrov for useful discussions. The support of the European Research Agency (FP7-PEOPLE-2009-IAPP Marie Curie IAPP transfer of knowledge programme, Project Reference No. 251475) is gratefully acknowledged.

References

[1] Economides M.J., Nolte K.G. Reservoir Stimulation. Prentice Hall, Englewood Cliffs, New Jersey, 1989.

[2] Adachi J., Siebrits E., Peirce A., Desroches J. Computer simulation of hydraulic fractures // Int. J. Rock Mech. Min. Sci., 44, 2007, pp. 739-757.

[3] Rutgers Ir.R. Relative viscosity of suspensions of rigid spheres in Newtonian liquids // Rheol. Acta, 2, 1962a, pp. 202–210.

[4] Rutgers Ir.R. Relative viscosity and concentration // Rheol. Acta, 2, 1962b, pp. 305–348.

[5] Thomas D.G. Transport characteristics of suspension: VIII. A note on the viscosity of Newtonian suspensions of uniform spherical particles // J. Coll. Sci., 20, 1965, pp. 267–277.

[6] Mueller S., Llewellin E.W., Mader H.M. The rheology of suspensions of solid particles // Proc. R. Soc. A, 466, 2010, pp. 1201–1228.

[7] Einstein A. Eine neue Bestimmung der Molekuldimensionen // Ann. Phys. 19, 1906, pp. 289–306.

[8] Brady J.F. The Einstein viscosity correction in n dimensions // Int. J. Mult. Flow, Vol. 10, Is. 1, 1983, pp. 113-–114.

[9] Nicomedo L., Nicolais L., Landelt R.F. Shear rate dependent viscosity of suspensions in Newtonian and non-Newtonian liquids // Chem. Eng. Sci., 1974, pp. 729–735.

[10] Dorr A., Sadiki A., Mehdizadeh A. A discrete model for the apparent viscosity of polydisperse suspensions including maximum packing fraction // arXiv:1202.3804v1 [physics.flu-dyn] (submitted to Physics of Fluids), 2012.

[11] Foss D.R., Brady J.F. Structure, diffusion, and rheology of Brownian suspensions by Stokesian dynamics simulations // J. Fluid. Mech., 407, 2000, pp. 167–200.

[12] Martys N.S. Study of a dissipative particle dynamics based approach for modeling suspensions // J. Rheol., 49, 2005, pp. 401–424.

[13] Martys N.S., George W.L., Chun B.-W., Lootens D. A smoothed particle hydrodynamics-based fluid model with a spatially dependent viscosity: application to flow of a suspension with a non-Newtonian fluid matrix // Rheol. Acta, Vol. 49, Is. 10, 2010, pp. 1059–1069.

[14] Wang Y., Keblinski P., Chen Z. Viscosity calculation of a nanoparticle suspension confined in nanochannels // Phys. Rev. E 86, 036313, 2012.

[15] Nguyen N-Q., Ladd A.J.C. Lubrication corrections for lattice-Boltzmann simulations of particle suspensions // Phys. Rev. E, 66, 046708, 2002.

[16] Ladd A.J.C., Colvin M.E., Frenkel D. Application of Lattice-Gas Cellular Automata to the Brownian Motion of Solids in Suspension // Phys. Rev. Let., Vol. 60, No. 11, 1988, pp. 975–978.

[17] Hoover W.G. Molecular dynamics, Lecture Notes in Physics, Vol. 258, Springer, Berlin, 1986, 138 p.

[18] Allen M.P., Tildesley D.J. Computer simulation of liquids, Clarendon Press, Oxford, 1987, 385 p.

[19] Kirvtsov A.M. Deformation and fracture of solids with microstructure. Moscow, Fizmatlit. 2007, 304 p. (In Russian)

[20] Monaghan J.J. Smoothed particle hydrodynamics // Rep. Prog. Phys. 68, 2005, pp. 1703–1759.

[21] Hoover W.G. Smooth Particle Applied Mechanics : The State of the Art. World Scientific Publishing, 2006, 316 p.

[22] Langston P.A., Al-Awamleh M.A., Fraige F.Y., Asmar B.N. Distinct element modelling of non-spherical frictionless particle flow // Chem. Eng. Sci. 59, 2, 2004, pp. 425–435.

[23] Kruggel-Emden H., Rickelt S., Wirtz S., Scherer V. A study on the validity of the multi-sphere Discrete Element Method // Powd. Tech., Vol. 188, No. 2, 2008, pp. 153-165.

[24] Cundall P.A., Strack O.D.L. A discrete numerical model for granular assemblies // Geotechnique, Vol. 29, No. 1, 1979, pp. 47–65.

[25] Berendsen H.J.C., Postma J.P.M., van Gunsteren W.F., Di Nola A., Haak J.R. Molecular-Dynamics with Coupling to an External Bath // J. Chem. Phys., 81, 8, 1984, pp. 3684–3690.

[26] Krivtsov A.M., Morozov N.F. Anomalies in Mechanical Characteristics of Nanometer-Size Objects // Doklady Physics, 46(11), 2001, pp. 825–827.

[27] Chapman S., Cowling T.G. The Mathematical Theory of Non-uniform Gases: An Account of the Kinetic Theory of Viscosity, Thermal Conduction and Diffusion in Gases. Cambridge University Press, 1995, 423 p.

Vitaly A. Kuzkin, Rzeszow University of Technology, Institute for Problems in Mechanical Engineering RAS
Anton M. Krivtsov, Rzeszow University of Technology, Saint Petersburg State Polytechnical University
Aleksandr M. Linkov, Rzeszow University of Technology, Saint Petersburg State Polytechnical University